Atmos. Meas. Tech. Discuss., 4, 1677–1721, 2011
www.atmos-meas-tech-discuss.net/4/1677/2011/
doi:10.5194/amtd-4-1677-2011

Atmospheric Measurement Techniques Discussions

Comparison of HDO measurements from Envisat/MIPAS with observations by Odin/SMR and SCISAT/ACE-FTS

S. Lossow[1], J. Steinwagner[2], J. Urban[3], E. Dupuy[4], C. D. Boone[5], S. Kellmann[1], A. Linden[1], M. Kiefer[1], U. Grabowski[1], M. Höpfner[1], N. Glatthor[1], T. Röckmann[2], D. P. Murtagh[3], K. A. Walker[6], P. F. Bernath[7], T. von Clarmann[1], and G. P. Stiller[1]

[1]Karlsruhe Institute of Technology, Institute for Meteorology and Climate Research, Hermann-von-Helmholtz-Platz 1, 76344 Leopoldshafen, Germany
[2]Utrecht University, Institute for Marine and Atmospheric Research Utrecht, Princetonplein 5, 3584 CC Utrecht, The Netherlands
[3]Chalmers University of Technology, Department of Earth and Space Science, Hörsalsvägen 11, 41296 Göteborg, Sweden
[4]National Institute of Information and Communications Technology (NICT), Applied Electromagnetic Research Center, 4-2-1 Nukui-kita, Koganei, Tokyo 184-8795, Japan
[5]University of Waterloo, Department of Chemistry, 200 University Avenue West, Waterloo, Ontario N2L 3G1, Canada

[6]University of Toronto, Department of Physics, 60 St. George Street, Toronto, Ontario M5S 1A7, Canada
[7]University of York, Department of Chemistry, Heslington, York, YO10 5DD, UK

Received: 11 February 2011 – Accepted: 8 March 2011 – Published: 11 March 2011

Correspondence to: S. Lossow (stefan.lossow@kit.edu)

Published by Copernicus Publications on behalf of the European Geosciences Union.

Abstract

Measurements of thermal emission in the mid-infrared by Envisat/MIPAS allow the retrieval of HDO information roughly in the altitude range between 10 km and 50 km. From September 2002 to March 2004 MIPAS performed measurements in the full spectral mode. To assess the quality of the HDO data set obtained during that period comparisons with measurements by Odin/SMR and SCISAT/ACE-FTS were performed. Comparisons were made on profile-to-profile basis as well as using seasonal and monthly means. All in all the comparisons yield favourable results. The largest deviations between MIPAS and ACE-FTS are observed below 15 km, where relative deviations can occasionally exceed 100%. Despite that the latitudinal structures observed by both instruments fit. Between 15 km and 20 km there is less consistency, especially in the Antarctic during winter and spring. Above 20 km there is a high consistency in the structures observed by all three instruments. MIPAS and ACE-FTS typically agree within 10%, with MIPAS mostly showing higher abundances than ACE-FTS. Both data sets show considerably more HDO than SMR. This bias can mostly be explained by uncertainties in spectroscopic parameters. Above 40 km, where the MIPAS HDO retrieval reaches its limits, still good agreement with the structures observed by SMR is found for most seasons. This puts some confidence in the MIPAS data at these altitudes.

1 Introduction

Water vapour is one of the fundamental constituents of the Earth's atmosphere. As the most important greenhouse gas in the troposphere and lower stratosphere any long-term change of its abundance in this altitude region will inevitably have important implications for the climate on Earth. But even changes in water vapour at higher stratospheric altitudes can significantly influence the surface climate (Forster and Shine, 1999; Solomon et al., 2010). Water vapour is also a main constituent of

AMTD
4, 1677–1721, 2011

polar stratospheric clouds (PSC). The heterogeneous chemistry that takes place on the cloud particle surfaces plays a decisive role for the severe ozone depletion that can be observed in the polar lower stratosphere during winter and spring time. At the same time water vapour is also the primary source of hydrogen radicals (HO_x = OH, H, HO_2) in the middle atmosphere. These radicals participate in the auto-catalytic cycles that destroy ozone with their contribution dominating above 50 km (Brasseur and Solomon, 2005).

Most water vapour resides in the troposphere. With increasing altitude the tropospheric concentrations typically decrease as the decreasing temperatures reduce the water vapour pressure and the distance to the major source regions, i.e. the oceans and land surfaces, increases. The entry of water vapour into the stratosphere occurs primarily through the cold tropical tropopause layer (TTL) where a large fraction of water vapour is removed due to freeze-drying. A large range of temporal and spatial scales are assumed to be of importance, still final consensus on the exact mechanisms and path ways behind the dehydration in the tropical tropopause region has not been reached. A secondary pathway of water vapour into the stratosphere is along isentropic surfaces that span both the uppermost troposphere and lowermost stratosphere (Holton et al., 1995). Overall the mean input of water vapour into the stratosphere amounts to about 3.5 ppmv–4.0 ppmv (e.g. Kley et al., 2000). In the stratosphere water vapour is produced by the irreversible oxidation of methane. This oxidation continues in the mesosphere but above 60 km this process stops to contribute significantly to the overall water vapour budget. An additional minor source in the upper stratosphere is the oxidation of molecular hydrogen (Wrotny et al., 2010). The main sink of water vapour in the stratosphere is the reaction with $O(^1D)$. Of small importance are dehydration effects by the sedimentation of PSC particles in the polar vortices (Kelly et al., 1989; Vömel et al., 1995). The interaction of the altitude-dependent water vapour production, destruction and transport processes leads to an increase of water vapour with altitude in the stratosphere. A local water vapour maximum is typically found around the stratopause indicating an equilibrium between all processes. In the mesosphere

AMTD
4, 1677–1721, 2011

no major water vapour source exists in general. Hence, the water vapour budget in this atmospheric layer is dominated by destruction processes, primarily photodissociation, resulting in a steady decrease of the water vapour abundance with increasing altitude.

The present work focuses on monodeuterated water vapour (HDO) in the stratosphere. Like the other minor water vapour isotopologues ($H_2^{17}O$, $H_2^{18}O$, HTO, $HD^{17}O$, D_2O, $HD^{18}O$, T_2O, ..., sorted by molar mass) HDO is several orders of magnitude less abundant than the main isotope $H_2^{16}O$ (hereafter H_2O). Scientifically HDO can be used as a tracer of dynamical processes in the middle atmosphere, however the main interest lies in the ratio of HDO with other isotopologues, typically with H_2O. This ratio can eventually provide more information than a single isotope alone. The standard convention to express the isotopic ratio between HDO and H_2O is the δD notation:

$$\delta\mathrm{D} = \left(\frac{R_{\mathrm{sample}}}{R_{\mathrm{reference}}} - 1 \right) \cdot 1000 \quad [\mathrm{unit}: \permil] \tag{1}$$

δD actually describes the relative deviation of the deuterium [D] to hydrogen [H] ratio $R = [D]/[H]$ with respect to the reference ratio $R_{\mathrm{reference}}$ which has been designated by the International Atomic Energy Agency in 1968 as $R_{\mathrm{reference}} = 155.76 \times 10^{-6}$ = VSMOW (Vienna Standard Mean Ocean Water). For the application of HDO and H_2O in the δD framework the following relation needs to be taken into account:

$$R_{\mathrm{sample}} = \left(\frac{[D]}{[H]} \right)_{\mathrm{sample}} \approx \left(\frac{[\mathrm{HDO}]}{2 \cdot [\mathrm{H_2O}]} \right)_{\mathrm{sample}} \tag{2}$$

A water vapour sample with 50% of its HDO removed would for example yield an isotopic ratio δD of $-500\permil$, if all HDO is removed then δD is $-1000\permil$. The dominating effect in the atmosphere influencing the $[D]/[H]$ ratio is the vapour pressure isotope effect. As HDO is heavier than H_2O it has a lower vapour pressure leading to a change in the isotopic ratio whenever a phase change occurs. For this reason the isotopic composition has been suggested as a valuable tool in determining the entry processes

AMTD
4, 1677–1721, 2011

and pathways of water vapour into the stratosphere (Moyer et al., 1996). This has stimulated numerous observational and model studies primarily aiming at the resolution of the long-standing debate on the relative importance of gradual ascent and convective processes to the stratospheric input of water vapour (e.g. Johnson et al., 2001b; Webster and Heymsfield, 2003; Kuang et al., 2003; Gettelman and Webster, 2005; Payne et al., 2007; Nassar et al., 2007; Hanisco et al., 2007; Steinwagner et al., 2010; Sayres et al., 2010). Measurements place the typical stratospheric entry value of δD in the range between −500‰ and −700‰. These values deviate from what is expected from the freeze-drying of air masses by gradual ascent alone (Rayleigh fractionation of ∼ −900‰), clearly indicating an involvement of convective processes. The isotopic ratio between HDO and H_2O has not only scientific relevance for the troposphere-stratosphere exchange but also in regions where polar stratospheric clouds occur. The limited number of observations as well as model efforts exhibit a significant influence of these clouds on the δD distribution (Stowasser et al., 1999; Ridal, 2001; Payne et al., 2007).

Air-borne measurements on campaign basis throughout 1978 and 2005 have indicated a decrease of δD in the air column above 13 km in the northern hemisphere (Coffey et al., 2006). This decrease is based on both a decrease in HDO and an increase in H_2O over this time period. The latter trend is consistent with other observations that show this temporal behaviour until about 2000 (Oltmans et al., 2000; Rosenlof et al., 2001; Scherer et al., 2008; Hurst et al., 2011). The trend in HDO remains unexplained even to date.

The low abundance of HDO has made its observation difficult and consequently the existing data base is limited. First observations of HDO in the altitude range of interest just date back to the late 1960s and 1970s employing a direct sampling technique (Scholz et al., 1970; Pollock et al., 1980). Over the years a number of balloon- and air-borne observations were performed, both in-situ and by means of remote sensing (e.g. Rinsland et al., 1984; Abbas et al., 1987; Dinelli et al., 1991; Zahn et al., 1998; Stowasser et al., 1999; Johnson et al., 2001a; Webster and Heymsfield, 2003;

AMTD
4, 1677–1721, 2011

Coffey et al., 2006; Hanisco et al., 2007; Sayres et al., 2010). These observations were generally made on a campaign basis covering limited spatial and temporal scales. The first space-borne observations were made by the ATMOS (Atmospheric Trace Molecule Spectroscopy, Farmer, 1987) Fourier transform spectrometer that was carried by the Space Shuttle during four missions (April/May 1985, April 1992, April 1993 and November 1994, Rinsland et al., 1991; Irion et al., 1996; Moyer et al., 1996; Kuang et al., 2003). From August 1996 to June 1997 the IMG (Interferometric Monitor for Greenhouse gases, Kobayashi et al., 1999) instrument on board ADEOS (Advanced Earth Observing Satellite) provided observations of HDO in the troposphere and the lowermost stratosphere in the extra-tropics using the nadir sounding technique. Since the new millennium the observations by Odin/SMR (Sub-Millimetre Radiometer, Murtagh et al., 2002), Envisat/MIPAS (Michelson Interferometer for Passive Atmospheric Sounding, Fischer et al., 2008) and SCISAT/ACE-FTS (Atmospheric Chemistry Experiment – Fourier Transform Spectrometer, Bernath et al., 2005) form the backbone of the HDO observations and other minor water vapour isotopologues in the stratosphere. In February 2001 the Swedish-led Odin satellite was launched. One year later the European Envisat (Environmental Satellite) started its operations, followed by the Canadian SCISAT (Science Satellite, also known as ACE mission) satellite in 2003. In the troposphere HDO data are currently available from observations by Envisat/SCIMACHY (Scanning Imaging Absorption Spectrometer for Atmospheric Chartography, Bovensmann et al., 1999) and Aura/TES (Tropospheric Emission Spectrometer, Beer et al., 2001) as well as the IASI (Infrared Atmospheric Sounding Interferometer, Clerbaux et al., 2007) instruments aboard the MetOp series of polar orbiting meteorological satellites operated by EUMESAT (European Organisation for the Exploitation of Meteorological Satellites) (Worden et al., 2007; Frankenberg et al., 2009; Herbin et al., 2009). Alongside with these new satellite observations also model simulations of water vapour isotopologues gained importance (e.g. Ridal, 2001; Gettelman and Webster, 2005; Schmidt et al., 2005; Zahn et al., 2006; Risi et al., 2008).

AMTD
4, 1677–1721, 2011

In this paper we present contemporary comparisons of Envisat/MIPAS HDO measurements with observations by Odin/SMR and SCISAT/ACE-FTS in order to assess the quality of the satellite data set in the stratosphere. In the next section the MIPAS data set and its characteristics are described. This includes a short overview of the mean annual distribution of HDO for different latitude bands. In Sect. 3 the Odin/SMR and SCISAT/ACE-FTS data sets are described and subsequently the comparison approach and results are presented. The outcome of the comparisons is discussed in Sect. 4.

2 Envisat/MIPAS observations of HDO

Carried by an Ariane-5 rocket Envisat was launched a into polar, sun-synchronous orbit on 1 March 2002 from the Guyana Space Centre in Kourou (French Guyana). The satellite orbits the Earth at an altitude of about 790 km 14 times a day, passing the equator shortly after 10:00 LT on the descending node. On the ascending node the equator crossing time is around 22:00 LT. The satellite carries 10 instruments observing the Earth and its atmosphere for investigations of a wide scientific spectrum. The MIPAS instrument is a cooled high-resolution Fourier transform spectrometer measuring thermal emission at the atmospheric limb. The instrument operates in five spectral bands in the range between 685 cm^{-1} and 2410 cm^{-1} (4.1 µm–14.6 µm) and uses a rearward viewing direction (Fischer et al., 2008).

2.1 Data set

MIPAS information on HDO are based on measurements in the spectral range between 1250.00 cm^{-1} and 1482.45 cm^{-1} (6.7 µm–8 µm). In this comparison we focus on the MIPAS observations that were performed with full spectral resolution, that is 0.035 cm^{-1} (unapodised). These observations cover the time period between September 2002 to March 2004. After that only measurements with a spectral resolution of

AMTD
4, 1677–1721, 2011

0.0625 cm^{-1} were possible due to problems with the movement of the interferometer reflectors. The measurements of interest here were performed in the "nominal observation mode" scanning the atmospheric limb between 6 km and 68 km. In this mode spectra at in total 17 tangent heights are taken (6 km to 42 km in 3 km steps, 42 km to 52 km in 5 km steps and 52 km to 68 km in 8 km steps). A whole scan takes 76 s corresponding to a horizontal sampling of roughly one scan per 500 km assuming a satellite velocity of about 7 km/s, when projected on the ground. The instantaneous field of view (FOV) of the MIPAS instrument is 3 km in the vertical and 30 km in the horizontal, i.e. perpendicular to the line of sight. While the latitudinal coverage of the Envisat orbit does not reach entirely to the poles, the MIPAS pointing system employs an azimuth mirror that is tilted off the orbital track to allow also measurements at the highest latitudes.

The HDO data set of interest here has been retrieved with the IMK/IAA processor, which is a joint effort by the "Institut für Meteorologie und Klimaforschung" (IMK) in Karlsruhe (Germany) and the "Instituto de Astrofísica de Andalucía" (IAA) in Granada (Spain). The retrieval employs a non-linear least square approach (von Clarmann et al., 2003) with a first-order Tikhonov-type regularisation (Tikhonov, 1963a,b; Tikhonov and Arsenin, 1977) to avoid unphysical oscillations in the derived profiles. The radiative transfer through the atmosphere is modelled by the KOPRA (Karlsruhe Optimized and Precise Radiative Transfer Algorithm) model (Stiller, 2000). Vertical profiles of HDO can be retrieved roughly in the altitude range from 10 km to 50 km. At the lower altitude end the opaqueness of the atmosphere determined by cloudiness, aerosols and increasing water vapour absorption limits the retrieval of HDO information from the measurements. The upper limit is set by the signal-to-noise ratio. Up to an altitude of 40 km the vertical resolution of the retrieved data is around 5 km–6 km and the random noise error of a single profile amounts to about 20% (Steinwagner et al., 2007). Above 40 km the vertical resolution degrades as a combined consequence of the coarser measurement grid and the aforementioned decrease in the signal-to-noise ratio. The random noise error deteriorates as well and therefore data averaging above 45 km is recommended

AMTD
4, 1677–1721, 2011

in order to get significant results. A more detailed description of the IMK/IAA retrieval of monodeuterated water vapour can be found in Steinwagner et al. (2007). In this comparison we utilise data derived with the latest HDO retrieval version V3O_HDO_5.

2.2 Distribution overview

As the number of global HDO data sets in the stratosphere is very limited the following subsection is dedicated to provide an introductory overview of the HDO distribution as observed by Envisat/MIPAS. Here the focus is on the annual distribution of HDO. Latitudinal cross sections will be shown later in the seasonal comparisons presented in Sect. 3.3. The individual panels of Fig. 1 show the mean annual variation for various latitude bins based on the MIPAS observations with full spectral resolution between September 2002 and March 2004. Please note that the time axis of the panels representing the mid- and polar latitudes has been adapted in a way so that the summer season occurs always in the middle of these panels. The individual data points in Fig. 1 describe a mean over 30 days. Those means have always been calculated around the first and the mid day of a given month. A mean is based on at least 25 individual measurements. Where this requirement was not fulfilled the mean was discarded (white areas). No smoothing has been applied to the data.

As evident from the panels in the two uppermost rows of Fig. 1 the "tape recorder" effect (Mote et al., 1996) dominates the annual variation of HDO in the lower stratosphere in the tropical region (Steinwagner et al., 2010). At an altitude of 18 km in the latitude band from 5°S – 5°N the MIPAS measurements show the lowest abundances during the boreal spring while the annual maximum can be observed in boreal autumn. From there the "tape recorder" signal is transported upwards by about 10 km per year. Higher up in the upper stratosphere clear signatures of the semi-annual oscillation can be observed in HDO, peaking after the solstices consistent with earlier observations of this feature in H_2O (Randel et al., 1998). The annual cycle in the mid-latitudes and polar region of stratospheric HDO is dominated by an annual component controlled by the annual cycle in the mean meridional circulation patterns. In the polar stratosphere

AMTD
4, 1677–1721, 2011

a displacement of the vertical HDO maximum from the stratopause towards lower altitudes can be observed during winter due to the subsidence inside the polar vortex. Higher up in the upper stratosphere the annual HDO maximum can be found after the summer season as known from H_2O measurements (Seele and Hartogh, 1999).

3 Comparison

The quality assessment of the MIPAS data set of monodeuterated water vapour primarily focuses on the stratosphere. The comparison of the MIPAS HDO data set with the Odin/SMR and SCISAT/ACE-FTS results relies basically on two approaches. The first approach uses profile-to-profile comparison on the basis of well-defined criteria for coincident measurements between the instruments. In addition we use analyses of linear fits and correlations based on seasonal means to test the internal consistency of HDO data sets included in the comparison. As complement we show a comparison of monthly mean profiles in the tropical region, which is of special scientific interest. In the following subsection the Odin/SMR and SCISAT/ACE-FTS HDO data sets are characterised.

3.1 Contributing instruments

3.1.1 Odin/SMR

Odin is Swedish-led satellite mission in co-operation with Canada, France and Finland. The satellite was launched on 20 February 2001 into a sun-synchronous and near-terminator orbit at an altitude of 600 km. When the satellite was launched it crossed the equator at 18:00 LT on the ascending node and at 06:00 LT on the descending node. These crossing times have shifted by almost an hour as the orbit altitude has gradually decreased due to atmospheric drag. The Sub-Millimetre Radiometer is one of two instrument on board the Odin satellite. It measures thermal emission at the atmospheric limb with a 1.1 m telescope in several frequency bands between 486 GHz and

AMTD
4, 1677–1721, 2011

581 GHz as well as around 119 GHz (Frisk et al., 2003). Measurements by Odin/SMR are nominally performed along the orbital track providing a latitude coverage between 82.5° S and 82.5° N. Since 2004, SMR performs also observations off the orbital track during certain seasons as permitted by sun angle constraints, allowing full coverage from pole to pole. HDO information is retrieved from measurements of the 490 GHz band that covers a HDO emission line that is centred at 490.597 GHz (Urban et al., 2007). Measurements of this band are not performed on a daily basis, but initially on 3–4 days per month. After a major rearrangement of the SMR measurement schedule in April 2007 the observation rate increased to 8–9 days a month. The 490 GHz band measurements are part of a stratosphere-mesosphere mode employing scans over the altitude range between 7 km and 110 km. With a scanning velocity of 0.75 km s^{-1} it takes almost 140 seconds to perform a complete limb scan. This translates into a horizontal sampling of approximately one scan per 1000 km. The integration time for an individual tangent view is approximately 1.85 s. Combined with the detector read-out times and the antenna characteristics the vertical sampling amounts to 3 km. The retrieval of HDO employs a non-linear scheme of the Optimal Estimation Method (OEM, Rodgers, 2000). HDO information can roughly be retrieved in the altitude range between 20 km and 70 km with an altitude resolution of 3 km to 4 km (Urban et al., 2004, 2007). The limiting factor at the lower altitude is due to the increasing water vapour absorption with decreasing altitude and limitations of the signal-to-noise ratio. This ratio determines also the upper altitude limit of the retrieval where the HDO emission line gets very narrow. The random noise error of a single profile retrieved is in the order of 20% to 40% in the altitude range between 20 km and 50 km, i.e. similar to the MIPAS data set. In the comparison we use data that has been processed with the latest official retrieval version 2.1 at the Chalmers University of Technology in Göteborg, Sweden.

3.1.2 SCISAT/ACE-FTS

The SCISAT (or SCISAT-1) satellite was launched on 12 August 2003 into a high inclination (74°) orbit with an altitude of 650 km providing overall a latitudinal coverage

AMTD
4, 1677–1721, 2011

between 85° S and 85° N. The orbit has been optimised for observations in the polar regions and mid- latitudes. Like Odin, the ACE mission carries two instruments on board. Similar to MIPAS, the ACE-FTS instrument is a high-resolution (i.e. 0.02 cm^{-1}) Fourier transform spectrometer that performs measurements over the spectral range between 750 cm^{-1} and 4400 cm^{-1} (2.3 µm to 13.3 µm). The instrument employs the solar-occultation technique measuring the attenuation of sunlight by the atmosphere during sunset and sunrise, yielding up to 30 observations per day. ACE-FTS scans the atmosphere in the altitude range between ~5 km and 150 km. The vertical sampling varies from around 1 km in the middle troposphere to roughly 2 km–3.5 km in the altitude range between 10 km and 20 km and to 5 km–6 km in the upper stratosphere and mesosphere. The instrument has a field of view of 1.25 mrad which coverts to about 3 km–4 km depending on altitude and observation geometry. HDO data is retrieved from spectral information in the wave number intervals between 1402.71 cm^{-1}–1497.97 cm^{-1} (6.7 µm–7.1 µm) and 2612.34 cm^{-1}–2672.80 cm^{-1} (3.7 µm–3.8 µm). In total, 24 microwindows are used. The data retrieval uses a "global-fit" approach (Carlotti, 1988) that employs an unconstrained Levenberg-Marquardt non-linear least-squares method. HDO information can typically be retrieved in the altitude range from 5.5 km to 37.5 km. The vertical resolution of this set of data is determined by the instrument's FOV and vertical sampling of the atmosphere, typically amounting to 3 km–4 km. The lower limit of the retrievals is determined mainly by cloudiness, while the uppermost retrieval altitude is determined by the signal-to-noise ratio of the measurements. The random noise error of an individual profile retrieved is in the order of 10%. In this comparison, we use the "HDO update" data set processed with the a slightly modified version of the original retrieval version 2.2 (Nassar et al., 2007).

AMTD
4, 1677–1721, 2011

3.2 Profile-to-profile comparisons

3.2.1 Methodology

For the profile-to-profile comparisons we consider observations by two instruments as coincident when they meet the following criteria: (1) a spatial separation of less than 500 km and (2) a temporal separation that does not exceed 6 h. These criteria represent a trade-off between a sufficient number of coincident measurements to draw significant conclusions and the avoidance of, in particular, spatial variations that could significantly influence the comparison. As the diurnal variation of HDO in the stratosphere is insignificant, a more relaxed time criteria could be used but tests showed that the results are virtually the same. In cases with multiple coincidences, the one located closest in space was used.

Prior to the comparison the data sets were screened to identify retrieved profiles or individual data points whose quality was not sufficient. In a first step this screening was based on the recommendations of the data processing teams. For the MIPAS data set this concerned the visibility flag and the averaging kernel diagonal criterion. For the retrieved data at a given altitude the visibility flag indicates interference by clouds based on the so-called cloud index (Spang et al., 2004). This index is ratio between the mean radiances in two spectral intervals of the measured spectra (788.20 cm^1–796.24 cm^1 versus 832.30 cm^1–834.4 cm^1). Investigations have shown that for any cloud index below 4 the presence of clouds cannot be excluded. In these cases the visibility flag is set to 0 and the retrieved data is omitted, effectively resulting in a clear sky bias. As a consequence the number of available data points typically decreases rapidly below the tropopause. In addition data have been used only if the diagonal element of the averaging kernel matrix exceeded an empirical threshold value of 0.03, ensuring that the retrieved data represents the state of the atmosphere and is not dominated by retrieval constraints. The Odin/SMR data set has been screened according to the retrieval quality flag and the measurement response to the retrieved values. The retrieval quality flag indicates if a profile shall be used for scientific analysis based on the cost function,

AMTD
4, 1677–1721, 2011

convergence and the regularisation of the retrieval along with the retrieved pointing offset. A measurement response of at least 70% was required in order to minimise the influence of the a priori information needed in the SMR OEM retrieval (e.g. Rodgers, 2000; Eriksson et al., 2005). With respect to the ACE-FTS data set data issues listed on the "Data Issues page" https://databace.uwaterloo.ca/validation/data_issues_table.php were taken into account and the affected data discarded. Negative concentrations were not filtered in this analysis as these values can be a result of the retrieval due to measurement noise, in particular at the hygropause and the lower and upper boundaries where retrievals are possible. Finally the data sets were inspected visually to remove data points with totally unphysical HDO abundances that remained after the previous filtering steps. Typically this concerned only a handful profiles of the individual data sets.

As the individual satellite data sets are provided on different altitude grids the coincident profiles were interpolated on a regular 1 km altitude grid for the comparison. The vertical resolution of the HDO profiles retrieved from the MIPAS measurements is somewhat lower than the vertical resolution of the ACE-FTS and SMR data. As for a large part of the stratospheric altitudes that are of concern here the HDO distribution is rather smooth so that the profiles can be compared directly despite those differences in the vertical resolution of the individual data sets. However in altitude layers where the HDO distribution is more structured, e.g. around the hygropause or stratopause, a direct comparison of the profiles may not always be appropriate and then the differences in the vertical resolution need to be taken into account. To study the influence of the different vertical resolutions on the comparison results the SMR and ACE-FTS profiles were degraded to the vertical resolution of the MIPAS profiles, following the method of Connor et al. (1994):

$$\hat{\mathbf{x}}_c = \mathbf{x}_a + \mathbf{A} \cdot (\hat{\mathbf{x}}_h - \mathbf{x}_a) \quad (3)$$

Here $\hat{\mathbf{x}}_c$ represents the degraded and $\hat{\mathbf{x}}_h$ the high vertically resolved SMR or ACE-FTS profile, while $\mathbf{x}_a$ and $\mathbf{A}$ describe the a priori profile and the averaging kernel matrix

AMTD
4, 1677–1721, 2011

of the MIPAS HDO retrieval, respectively. The reader may be reminded at this point that in the MIPAS retrieval the a priori profile serves only the purpose of constraining the shape or smoothness of a retrieved profile, different to the OEM approach were the a priori profile is also used to constrain the retrieved abundances. The coincident profiles from SMR and ACE-FTS were only compared directly as their vertical resolutions are very similar in the altitude range where these two data sets overlap.

The bias B between two coincident data sets nos. 1 and 2 comprising n coincidences is calculated as:

$$B = \frac{1}{n} \cdot \sum_{i=1}^{n} b_i \tag{4}$$

where b_i denotes the difference between each individual pair of coincident data points:

$$b_i = \hat{x}_{1,i} - \hat{x}_{2,i} \tag{5}$$

in which $\hat{x}$ refers to the retrieved HDO data from the individual data sets. To express the deviation in relative terms we use the following relation:

$$b_i = b_{i,\mathrm{rel}} = \frac{\hat{x}_{1,i} - \hat{x}_{2,i}}{(\hat{x}_{1,i} + \hat{x}_{2,i})/2} \tag{6}$$

This is based on the assumption that satellite measurements might have large uncertainties, so that it is more convenient to refer to the mean of the two data sets involved rather than to one specific data set (e.g. Randall et al., 2003; Dupuy et al., 2009). Additional information on the comparison is supplied in form of the de-biased standard deviation and the standard error of the mean (SEM). The de-biased standard deviation σ is represented by the standard deviation of the bias-corrected deviations between two data sets compared:

$$\sigma = \sqrt{\frac{1}{n-1} \cdot \sum_{i=1}^{n} (b_i - B)^2} \tag{7}$$

AMTD
4, 1677–1721, 2011

This quantity serves as a measure of the combined precision of the two data sets that are compared (von Clarmann, 2006), particularly in cases where a complete random error budget assessment is not available for all involved instruments, as in the present study. The standard error of the mean provides information on the significance of the derived bias between two data sets and is calculated as:

$$\mathrm{SEM} = \frac{\sigma}{\sqrt{n}} \tag{8}$$

Finally it should be noted that all variables given in Eqs. (4) to (8) are implicitly dependent on altitude, that means that the bias B for example refers to the bias at a given altitude.

3.2.2 Results

Figure 2 shows the results of the profile-to-profile comparisons between MIPAS and ACE-FTS (upper panels), MIPAS and SMR (middle panels) and SMR and ACE-FTS (lower panels). The panels on the left-hand side show the mean profiles based on the coincident pairs of data. These panels contain on the left information on the number of coincident profiles as well as their average separation in terms of time, distance, latitude and longitude. On the right the number of coincident pairs at a given altitude are indicated every 3 km. The middle panels show the biases between the coincident data sets in absolute terms, in the panels on right-hand side the relative biases are presented by solid lines in each case. In these two panels the results of direct comparisons are shown in black, if the vertical resolution of one data set has been degraded the results are given in green. The dash-dotted lines represent the estimated combined precision of the compared data sets on the basis of the de-biased standard deviation σ, comprising contributions from the measurement noise and the small temporal and spatial mismatch of the coincidences. The dashed lines indicate the standard error of the bias according to Eq. (8). The reader may be reminded at this point that the absolute and relative bias is calculated from each individual pair of coincident profiles which

AMTD
4, 1677–1721, 2011

can lead to some apparent discrepancies in the comparison between mean profiles, as visible in Fig. 2.

Based on the coincidence criteria defined in Sect. 3.2.1 we found 140 pairs of coincident observations of MIPAS and ACE-FTS which on average were separated by almost 5 h in time and 250 km in distance. As the ACE-FTS commissioning phase just ended in January 2004 and the MIPAS measurements with full spectral resolution ceased in March 2004 the temporal overlap between both data sets is very limited. During the overlap period the ACE-FTS observations were focusing on the Arctic. A majority of the coincident measurements occurred in the latitude range between 75° N and 80° N, while the lowest latitude was 55° N. The comparison for this limited period of time and region exhibits a favourable result. The deviations are typically smaller than 0.1 ppbv or 10% and well within the estimated precision boundaries. Exceptions can be found at the lower and upper altitude end where comparisons were possible. Here also the significance of the derived bias decreases. Degrading the ACE-FTS data onto the altitude resolution of MIPAS clearly improves the comparison result at these altitudes. For most altitudes the MIPAS observations show higher concentrations than the coincident measurements by ACE-FTS. There is a prominent oscillation in the bias between 15 km and 30 km. The consistency between both data sets does not change significantly when the comparison is made separately for the polar vortex inside and outside.

The profile-to-profile comparison between MIPAS and SMR covers almost the entire time period in which the full spectral resolution measurements by MIPAS were possible, i.e. coincidences were found throughout October 2002 to February 2004. The results shown in Fig. 2 represent the global average over all coincidence cases. Most of those where found in the polar regions with a decreasing number towards the tropics. In the month domain the highest number of coincident measurements could be obtained in December however none in March, May and August. On the global average the SMR data set exhibits a dry bias compared to the MIPAS data at all altitudes addressed here. The results are almost identical for the direct comparison and the comparison

AMTD
4, 1677–1721, 2011

using SMR data that have been degraded to the vertical resolution of MIPAS. The bias maximises below 20 km with values between 0.25 ppbv and 0.4 ppbv or more than 80% in relative terms. This bias can be attributed to a substantial fraction of data with large random noise errors. Between 17 km and 20 km 20% to 50% of the data exhibits relative errors larger than 100%, below 17 km the fraction is even higher. From 20 km to 50 km the bias decreases gradually from 0.25 ppbv to nearly a half of that. The relative bias decreases from about 60% at 20 km to less than 10% at 50 km. Looking at different seasons and latitude bands does not change the overall picture clearly indicating that the bias is a systematic feature (not shown here).

Similar structures that were visible in the comparison between MIPAS and SMR can also be observed when coincident observations of ACE-FTS and SMR are compared with each other. Above 20 km the SMR observations show again a low bias of about 0.2 ppbv to 0.25 ppbv compared to the ACE-FTS measurements on a global scale. Coincident measurements between February 2004 and August 2009 were implemented in the comparison. Because of the optimisation of SCISAT orbit, the bulk of the coincidences were found in the mid-latitudes and polar regions. Most coincident measurements of both instruments were available around the equinoxes.

3.3 Seasonal comparisons

3.3.1 Methodology

In this section we consider comparisons for the individual seasons in the latitudinal plane. For this the data sets were averaged over latitude bins of 10° centred at 85° S, 75° S, ..., 75° N and 85° N for the individual seasons, i.e. MAM (March, April and May), JJA (June, July and August), SON (September, October and November) and DJF (December, January and February). As for the annual distributions shown in Fig. 1 25 measurements were required for a mean to be considered in order to avoid spurious data points in the latitudinal cross sections. The data were again interpolated

AMTD
4, 1677–1721, 2011

on a regular vertical grid of 1 km. For the MIPAS and SMR data sets we considered the time period between September 2002 and February 2004, meaning that boreal autumn and winter are sampled twice. As ACE-FTS observations just started in 2004 we chose the time periods from September 2004 to February 2006 and from September 2006 to February 2008 instead. The choice of two time periods was motivated by the smaller number of observations by ACE-FTS as compared to the other instruments due to the utilisation of the solar occultation technique. These particular periods were selected with regard to the phase of the quasi-biennial oscillation (QBO), which was quite similar for all three time periods employed, i.e. the QBO period was rather close to 24 months during these years. A third possible time period from September 2008 to February 2010 was disregarded because the QBO cycle exhibited clearly a much longer period than before. Overall the choice of the ACE-FTS time periods will minimise the influence of QBO effects on the results of the seasonal comparison. However there is still a possibility that the comparison of the ACE-FTS results with the other two instruments might be affected by any change in the temporal behaviour of HDO throughout the time periods considered. Opposite to profile-to-profile comparisons the SMR and ACE-FTS were not degraded to the vertical resolution of the MIPAS retrieval. On the one hand it is difficult to provide the appropriate convolution data for an entire dataset, on the other hand the data averaging tends to reduce the differences in the vertical resolution among the individual data set.

To describe the significance of the derived cross section we use as for the biases in the profile-to-profile comparisons the SEM. For the particular application here the standard error is denoted as ϵ and derived as follows:

$$\epsilon = \sqrt{\frac{1}{k \cdot (k-1)} \cdot \sum_{i=1}^{k} \left(\hat{x}_i - \overline{\hat{x}}\right)^2} \tag{9}$$

k describes the number of retrieved data points $\hat{x}$ of an individual data set that fall into a given latitude bin for a specific season and altitude. $\overline{\hat{x}}$ denotes the average over the entire ensemble of these data points. To characterise the consistency of the latitudinal

AMTD
4, 1677–1721, 2011

cross sections derived from two instruments at a given altitude and season we provide the parameter of a linear fit and the correlation coefficient. For the determination of the linear fit parameter a (intercept) and b (slope) an iterative scheme was employed to minimise the following regression relation:

$$\sum_{i=1}^{I} \frac{(x_{1,i} - a - b \cdot x_{2,i})^2}{\epsilon_{1,i}^2 + (b \cdot \epsilon_{2,i})^2}. \quad (10)$$

This relation considers the standard error ϵ (Eq. 9) that is associated with the averages x for a given season and latitude bin for the data sets nos. 1 and 2. I denotes the number of latitude bins. The correlation coefficients r were calculated by:

$$r = \frac{\sum_{i=1}^{I}(x_{1,i} - \overline{x}_1) \cdot (x_{2,i} - \overline{x}_2)}{\sqrt{\sum_{i=1}^{I}(x_{1,i} - \overline{x}_1)^2 \cdot (x_{2,i} - \overline{x}_2)^2}} \quad (11)$$

$\overline{x}$ describes the mean over all latitude bins for a given season for the individual data sets. The calculation of the correlation coefficients here does not consider any error estimates. We do not want to prove if two data sets are correlated by chance but simply show that the expected high correlation between the latitudinal cross sections observed by two instruments is present. As before all given variables are implicitly depending on altitude.

3.3.2 Results

Figure 3 and 4 present the latitudinal cross sections for the different seasons that were derived from the individual measurements. Figure 3 focuses on altitudes from 12 km to 24 km while Fig. 4 addresses altitudes above. The dashed lines represent the standard error of the cross sections. Typically between 1000 to 3000 individual MIPAS measurements contributed to the average for a given latitude bin, altitude and

AMTD
4, 1677–1721, 2011

season (lowest numbers in MAM and JJA as well as at the lowest altitudes). This is in general a factor of 10 more than for SMR and ACE-FTS. The latitudinal distribution observed by MIPAS and ACE-FTS at 12 km are fairly consistent during all seasons. Still, in relative terms, the deviations (referenced to the mean of both data sets) can amount up to 100% especially in MAM and JJA with ACE-FTS typically showing higher abundances. In 15 km also a good consistency can be found between the MIPAS and ACE-FTS data set. The relative deviations are typically within 30%. Higher up at 18 km the SMR observations contribute also to the comparisons, exhibiting larger variations in the latitudinal cross section as compared to the other data sets and even negative values can be observed in JJA. However the overall distribution is similar, but the absolute deviations can exceed 0.4 ppbv. The MIPAS and ACE-FTS latitudinal cross sections fit best in MAM. In JJA and SON deviations between these data sets occur noticeable in the Antarctic. There the ACE-FTS observations exhibit a pronounced drop in the HDO concentrations, while MIPAS and SMR observations agree quantitatively. Deviations between MIPAS and ACE-FTS are also evident in the tropics especially in JJA and DJF. Otherwise the agreement between the MIPAS and ACE-FTS concentration is typically within 20%. The latitudinal structures observed by all instruments at 24 km and 30 km exhibit in total a high degree of consistency. For the most part the MIPAS concentrations are slightly higher than those of ACE-FTS as previously seen in the profile-to-profile comparison in Fig. 2. The relative deviations between those two data sets typically do not exceed 10% at these altitudes. The absolute deviations between MIPAS and SMR at 30 km are on average slightly lower than 0.2 ppbv. This average deviation is smaller than at 24 km (0.24 ppbv) but also somewhat smaller than at 36 km (0.21 ppbv), thus deviating to some extent from the results obtained by means of the profile-to-profile comparison. Apart from that the uniformity in the latitudinal distributions observed by all instruments at 24 km and 30 km continues at 36 km. In SON more pronounced deviations between MIPAS and ACE-FTS can be observed in the southern hemisphere tropical and mid-latitudes. The differences between MIPAS and the SMR data set decrease noticeably in terms of absolute concentrations compared

AMTD
4, 1677–1721, 2011

to the lower altitudes. With the exception of MAM at 48 km the latitudinal structures remain to fit favourably. During this season SMR exhibits also higher concentrations than MIPAS in some latitude bins.

Example scatter plots using the average HDO concentrations for different latitude bins for all possible instrument combinations and seasons are shown in Fig. 5. Here the altitudes 18 km (lower panels), 30 km (middle panels) and 42 km (upper panels) are shown. Comparisons between MIPAS and ACE-FTS are given by blue data points, red data points show the comparison between MIPAS and SMR and green data points are used for the comparison between SMR and ACE-FTS. The data set named first uses the abscissa of the graph while the data set named last uses the ordinate. Small error bars around the data points indicate the standard error of the data. The solid lines represent the linear fits to the scatter data and the black dashed line indicates the ideal fit (intercept = 0, slope = 1). The comparisons at 18 km are influenced by scatter resulting in linear fits that deviate from the ideal case. In JJA the least agreement between the MIPAS and ACE-FTS latitudinal cross sections can be observed. Higher up the scatter is significantly reduced and the linear fits witness the overall good consistency between the individual data sets as evident from the previous figures. Figure 6 summarises quantitatively the results of the linear fit analysis for the altitude range between 10 km and 50 km. In addition the correlation coefficients are shown in the right panels. The latitudinal cross sections of MIPAS and ACE-FTS compare very well above 20 km showing linear fit parameters that are close to an ideal fit. The correlations coefficients are almost everywhere above 0.9 in this altitude region. High correlation coefficients can also be observed between 10 km and 15 km. There is a pronounced drop of the correlations in the altitude region from about 15 km to 20 km. This feature is characteristic for all comparisons between the individual instruments. The MIPAS and SMR latitudinal cross sections correlate nicely from about 20 km to 45 km. Above, high correlations can even be seen for JJA and DJF, while especially for MAM the consistency is significantly reduced as also evident from the line fit parameters. As for the other comparisons high correlation coefficients can be observed above 20 km during

AMTD
4, 1677–1721, 2011

all seasons when the latitudinal cross sections derived from the SMR and ACE-FTS measurements are compared.

3.4 Monthly comparisons in the tropics

In this comparison we focus on four months, namely February, April, August and October. Only in these months ACE-FTS observations cover the tropics as the ACE orbit is optimised for polar and mid-latitudes. Hence seasonal comparisons with ACE-FTS may be less appropriate in the tropics. For this comparison the data were averaged over the latitude range from 15° S to 15° N for a given month, considering data from the same time periods as used in the seasonal comparisons for the individual instruments (see Sect. 3.3.1). As before 25 measurements were required for a mean to be considered. Like for the seasonal comparisons ACE-FTS and SMR data were not degraded to the vertical resolution of the MIPAS data set. Figure 7 shows the tropical monthly mean profiles in the altitude region between 10 km and 50 km. The dashed lines represent the standard error of the mean profiles. In February the MIPAS observations exhibit rather constant volume mixing ratios around 20 km, while the SMR and ACE-FTS measurements show a distinct hygropause at 18 km. The bias between the SMR and ACE-FTS observations is here much smaller than particularly in the altitude range between 20 km and 25 km. Here the SMR observations exhibit a very structured HDO distribution, comprising a local maximum at 22 km and a local minimum close to 25 km. A similar structure is evident in the ACE-FTS observations, but the extrema are less pronounced. Above 30 km the bias between SMR and the other observations clearly decreases as seen in the earlier comparisons. A nice agreement in the vertical structures observed by all instruments is found in April, with a rather constant low bias by SMR compared to MIPAS and ACE-FTS. The hygropause is located at 18 km to 19 km. As in February the SMR observations exhibit a local maximum around 22 km and a local minimum higher up at about 25 km. The same features are also visible in the other observations, but for MIPAS at slightly different altitudes. In August the SMR and MIPAS measurements exhibit both a sharp hygropause structure, but the difference

AMTD
4, 1677–1721, 2011

between these data sets amounts to more than 0.4 ppbv at this altitudes. In the ACE-FTS observations the hygropause is rather smooth and located higher up compared to the other instruments. As in the previous months the SMR observations show distinct structures in the altitude range between 20 km and 30 km, the local extrema however are located somewhat higher up than in February and April, as consequence of the upward transport of the "tape recorder" signal. While the volume mixing ratios observed by ACE-FTS during this month are rather constant in the altitude range between 24 km and 30 km, the MIPAS observations exhibit a slight increase above 25 km. Around 35 km the bias between the ACE-FTS and SMR observations is smaller as the bias between MIPAS and ACE-FTS. In October the MIPAS and ACE-FTS observations exhibit the hygropause at 21 km. The ACE-FTS profile less structured than the MIPAS profile in the altitude range between roughly 18 km and 35 km. The hygropause in the SMR observations occurs below 20 km. No local extrema are observed above 20 km where the shape of the profile is rather similar to ACE-FTS. The bias between SMR and MIPAS is quite constant between 20 km and 35 km, decreasing considerably at higher altitudes as typical for all monthly comparisons considered here.

4 Summary and discussion

To assess the quality of the MIPAS HDO data set obtained with full spectral resolution from September 2002 to March 2004 comparisons with observations by Odin/SMR and SCISAT/ACE-FTS were performed. Overall the comparisons show favourable results, with very good consistency above 20 km and larger deviations at altitudes below.

The comparisons between MIPAS and ACE-FTS exhibit the largest deviations, both in absolute and relative terms, at the lowermost altitudes addressed here, i.e. below 15 km. At some latitudes the seasonal comparisons show relative deviations of more than 100%, even if there is overall a good consistency in the latitudinal structures observed by the two instruments. At 12 km the average relative deviation in the seasonal comparisons between MIPAS and ACE-FTS amounts to more than 40%. The

AMTD
4, 1677–1721, 2011

differences in the vertical resolution of the MIPAS and ACE-FTS are largest at these low altitudes, which might affect the results of the seasonal comparisons. Still the profile-to-profile comparisons accounting for these differences also show the largest deviations between the two data sets below 15 km. With increasing altitude the deviations between MIPAS and ACE-FTS decrease. At 15 km both data sets typically agree within 30% in the seasonal comparisons, at 20 km the relative deviation is on average about 10%. Yet a pronounced difference in the latitudinal distributions observed by MIPAS and ACE-FTS can be seen in the Antarctic in JJA and SON. Here the ACE-FTS observations exhibit a significant drop in the HDO abundances in the altitude range between about 15 km and 23 km. This feature is barely visible in the MIPAS (or SMR) observations, the relative deviations compared to ACE-FTS rising up to about 50% at 20 km. As the very same characteristics are evident in a corresponding seasonal comparison of H_2O (not shown here) it is natural to assume an influence from polar stratospheric clouds that occur at this location and time of year; likely due to dehydration effects from those PSC that are made of water ice (type II) (Kelly et al., 1989; Vömel et al., 1995). As different time periods were used to compile the latitudinal cross sections for MIPAS and ACE-FTS, pronounced differences in the PSC behaviour during these time periods may provide an explanation for this behaviour. Temperature analyses based on ECMWF (European Centre for Medium-range Weather Forecast) indicate more favourable conditions for the formation of PSC type II during the periods used for the ACE-FTS latitudinal cross section, especially in 2005 (not shown here). Still it is questionable if this can explain all differences. Most of the ACE-FTS data that goes into the seasonal averages of JJA and SON polewards of 70° S is obtained in August and September. Accounting for that by using monthly means instead reduces the deviations between the MIPAS and ACE-FTS data in September but not in August. Larger deviations between MIPAS and ACE-FTS can also be observed in February and August in the upper part of the TTL and slightly above. Differences in the vertical resolution of the HDO data sets from the MIPAS and ACE-FTS observation still might play a role here. However the largest uncertainties arise from clouds in the tropical

AMTD
4, 1677–1721, 2011

tropopause layer. MIPAS and ACE-FTS have a clear sky bias in this altitude region, while SMR is less affected by clouds as it uses spectral information in the microwave region. MIPAS and ACE-FTS share spectral information to derive HDO data, but different measurement techniques are employed. Differences in the applied cloud filtering can be of importance. Also the cloud filtering can influence altitudes higher up as the information that goes into the retrieval is changed. Steinwagner et al. (2010) performed a sensitivity study in which they intentionally omitted data from tangent heights that the cloud detection scheme (Spang et al., 2004) would allow for scientific use. They found a small dependence between the minimum tangent height included in the MIPAS retrieval and the mean profile derived from the test data set. In the upper part of the TTL virtually no influence was found, but around 21 km the influence amounted to about 0.025 ppbv. The influence of minimum tangent height on the mean profile continued up to about 25 km. Finally there are some spatial and temporal differences in the observations from the individual instruments that might an influence too. It is therefore rather unlikely that the satellite instruments see the same aspects of a cloudy scene and the associated HDO distribution. Nonetheless there is good agreement in the vertical structures observed in the tropics by all instruments between 20 km and 30 km where the "tape recorder" signal is transported upwards. The vertical distribution is more structured in the SMR observations than in the other measurements, likely because SMR has overall the best vertical resolution resolution in this altitude region for all instruments.

Above 20 km the MIPAS and ACE-FTS observations agree not only favourably in the tropics but also at the other latitudes. Up to 37 km where the current ACE-FTS HDO retrievals stop (future versions will extend into the 40 km to 50 km region) the HDO abundances typically agree within 10% (on average ~5%) for all seasons. In the majority of cases the MIPAS concentrations are on the high side. The comparison between MIPAS and SMR above 20 km reveal a dry bias of the SMR measurements which slowly decreases with altitude. Up to about 30 km the bias is typically between 0.2 ppbv and 0.3 ppbv during all seasons except for the latitude range between 20° S

AMTD
4, 1677–1721, 2011

and 20° N (below 25 km) where smaller deviations can be observed. Between 30 km and 35 km the bias exhibits a local minimum on average somewhere between 0.15 ppbv and 0.2 ppbv. Above 40 km the bias decreases most pronounced in the tropics to values around 0.1 ppbv while in the Antarctic region in MAM and JJA again an increase can be observed. To understand the reasons for this bias of the SMR data set compared to the other instruments, a quick sensitivity study with the SMR retrieval has been performed. This sensitivity study pointed towards the typical candidates, i.e. calibration and spectroscopic parameter, most important the line broadening parameter. Assuming an uncertainty of 5% in the line broadening parameter of the 490 GHz HDO emission line translates to an uncertainty of 0.05 ppbv in the retrieved data in the altitude range between 20 km and 50 km (Urban et al., 2004). Worst case estimates of the uncertainty of the line broadening parameter based on the HITRAN (High Resolution Transmission) spectroscopy database are considerably higher, explaining a large fraction of the bias observed. On the other hand the MIPAS and ACE-FTS retrievals of HDO use the same spectroscopic information and related errors. Ultimately any error in the shared spectroscopic parameters will change the comparison result with respect to the SMR data set. Uncertainties in the line intensities and pressure broadening lead to an uncertainty of more than 0.05 ppbv at 20 km in the MIPAS retrieval (Steinwagner et al., 2007). At 30 km the uncertainty is about 0.1 ppbv, at 40 km 0.15 ppbv. Thus, spectroscopic data play likely the dominant role in understanding the bias observed between SMR and the other instruments. Aside from the bias, the linear fit and correlation analysis of the latitudinal cross sections clearly indicates that a high degree of consistency exists in the structures observed among all three data sets that are compared here. This consistency above 20 km will be beneficial for further comparisons of structures in δD where the consistency will also rely on the quality of the observations of the main water vapour isotope. In addition the comparisons with SMR allow the quality of the MIPAS data above 42 km to be judged, where the statistical error of the retrieved data significantly increases. This comparison exhibits a good agreement for SON and DJF, to a large extent also for JJA. Good consistency is also found in

AMTD
4, 1677–1721, 2011

temporal structures as function of various latitude bins (not shown here). This puts some confidence into the MIPAS data set at these altitudes, however averaging over a larger set of observations is a prerequisite for scientific analyses.

5 Conclusions

The quality assessment of the MIPAS data set of monodeuterated water vapour has revealed favourable results. Above 20 km the MIPAS and ACE-FTS data sets agree quantitatively within 10%, while both instruments exhibit significantly higher concentrations than SMR. This bias can mostly be explained by uncertainties in spectroscopic parameters. Still the latitudinal structures for different seasons exhibit a high degree of consistency among all data sets, making this bias less an issue. Some confidence has also been raised for the MIPAS data set covering the altitude range between 42 km and 50 km. The largest deviations between the data sets can be found below 20 km, for some latitude bins the relative deviation between MIPAS and ACE-FTS exceeds 100% below 15 km. Still the latitudinal structures observed by both instruments fit at these altitudes. Higher up, between 15 km and 20 km, there is less consistency, especially in the Antarctic during winter and spring.

Acknowledgements. This work has been funded by the German Federal Ministry of Education and Research (BMBF) via contract no. 50 EE 0901. J. Steinwagner and T. Röckmann were financially supported by the Dutch Science foundation NWO (grant number ALW-GO-AO/07-01). We would like to thank the European Space Agency (ESA) for making the MIPAS level-1b data set available. Odin is a Swedish-led satellite project funded jointly by the Swedish National Space Board (SNSB), the Canadian Space Agency (CSA), the National Technology Agency of Finland (Tekes) and the Centre National d'Etudes Spatiales (CNES) in France. The Swedish Space Corporation has been the industrial prime constructor. Since April 2007 Odin is a third-party mission of ESA. The Atmospheric Chemistry Experiment (ACE), also known as SCISAT, is a Canadian-led mission mainly supported by the Canadian Space Agency (CSA) and the Natural Sciences and Engineering Research Council of Canada (NSERC). The MIPAS retrievals were partly performed on the HP XC4000 of the KIT Steinbuch Centre for Computing (SCC)

AMTD
4, 1677–1721, 2011

under the project grant MIPAS. The main author thanks C. Martin, J. Buckland, G. Berryman and W. Champion for their support.

References

Abbas, M. M., Guo, J., Carli, B., Mencaraglia, F., and Bonetti, A.: Stratospheric O_3, H_2O, and HDO distributions from balloon-based far-infrared observations, J. Geophys. Res., 92, 8354–8364, doi:10.1029/JD092iD07p08354, 1987. 1682

Beer, R., Glavich, T. A., and Rider, D. M.: Tropospheric emission spectrometer for the Earth Observing System's Aura satellite, Appl. Optics, 40, 2356–2367, doi:10.1364/AO.40.002356, 2001. 1683

Bernath, P. F., McElroy, C. T., Abrams, M. C., Boone, C. D., Butler, M., Camy-Peyret, C., Carleer, M., Clerbaux, C., Coheur, P.-F., Colin, R., DeCola, P., DeMazière, M., Drummond, J. R., Dufour, D., Evans, W. F. J., Fast, H., Fussen, D., Gilbert, K., Jennings, D. E., Llewellyn, E. J., Lowe, R. P., Mahieu, E., McConnell, J. C., McHugh, M., McLeod, S. D., Michaud, R., Midwinter, C., Nassar, R., Nichitiu, F., Nowlan, C., Rinsland, C. P., Rochon, Y. J., Rowlands, N., Semeniuk, K., Simon, P., Skelton, R., Sloan, J. J., Soucy, M.-A., Strong, K., Tremblay, P., Turnbull, D., Walker, K. A., Walkty, I., Wardle, D. A., Wehrle, V., Zander, R., and Zou, J.: Atmospheric Chemistry Experiment (ACE): Mission overview, Geophys. Res. Lett., 32, L15S01, doi:10.1029/2005GL022386, 2005. 1683

Bovensmann, H., Burrows, J. P., Buchwitz, M., Frerick, J., Noël, S., Rozanov, V. V., Chance, K. V., and Goede, A. P. H.: SCIAMACHY: Mission objectives and measurement modes, J. Atmos. Sci., 56, 127–150, doi:10.1175/1520-0469(1999)056¡0127:SMOAMM¿2.0.CO;2, 1999. 1683

Brasseur, G. and Solomon, S.: Aeronomy of the middle atmosphere, Springer, ISBN-10 1-4020-3284-6, P.O. Box 17, 3300 AA Dordrecht, The Netherlands, 2005. 1680

Carlotti, M.: Global-fit approach to the analysis of limb-scanning atmospheric measurements, Appl. Optics, 27, 3250–3254, 1988. 1689

Clerbaux, C., Hadji-Lazaro, J., Turquety, S., George, M., Coheur, P. F., Hurtmans, D., Wespes, C., Herbin, H., Blumstein, D., Tournier, B., and Phulpin, T.: The IASI/MetOp mission: first ob-servations and highlight of its potential contribution to the GMES Earth observation component, Space Research Today, 168, 19–24, 2007. 1683

AMTD
4, 1677–1721, 2011

Coffey, M. T., Hannigan, J. W., and Goldman, A.: Observations of upper tropospheric/lower stratospheric water vapor and its isotopes, J. Geophys. Res., 111, D14313, doi:10.1029/2005JD006093, 2006. 1682, 1683

Connor, B. J., Siskind, D. E., Tsou, J. J., Parrish, A., and Remsberg, E. E.: Ground-based microwave observations of ozone in the upper stratosphere and mesosphere, J. Geophys. Res., 99, 16757–16770, doi:10.1029/94JD01153, 1994. 1691

Dinelli, B. M., Carli, B., and Carlotti, M.: Measurement of stratospheric distributions of H2O-16, H2O-18, H2O-17, and HDO-16 from far infrared spectra, J. Geophys. Res., 96, 7509–7514, doi:10.1029/90JD02665, 1991. 1682

Dupuy, E., Walker, K. A., Kar, J., Boone, C. D., McElroy, C. T., Bernath, P. F., Drummond, J. R., Skelton, R., McLeod, S. D., Hughes, R. C., Nowlan, C. R., Dufour, D. G., Zou, J., Nichitiu, F., Strong, K., Baron, P., Bevilacqua, R. M., Blumenstock, T., Bodeker, G. E., Borsdorff, T., Bourassa, A. E., Bovensmann, H., Boyd, I. S., Bracher, A., Brogniez, C., Burrows, J. P., Catoire, V., Ceccherini, S., Chabrillat, S., Christensen, T., Coffey, M. T., Cortesi, U., Davies, J., de Clercq, C., Degenstein, D. A., de Mazière, M., Demoulin, P., Dodion, J., Firanski, B., Fischer, H., Forbes, G., Froidevaux, L., Fussen, D., Gerard, P., Godin-Beekmann, S., Goutail, F., Granville, J., Griffith, D., Haley, C. S., Hannigan, J. W., Höpfner, M., Jin, J. J., Jones, A., Jones, N. B., Jucks, K., Kagawa, A., Kasai, Y., Kerzenmacher, T. E., Kleinböhl, A., Klekociuk, A. R., Kramer, I., Küllmann, H., Kuttippurath, J., Kyrölä, E., Lambert, J., Livesey, N. J., Llewellyn, E. J., Lloyd, N. D., Mahieu, E., Manney, G. L., Marshall, B. T., McConnell, J. C., McCormick, M. P., McDermid, I. S., McHugh, M., McLinden, C. A., Mellqvist, J., Mizutani, K., Murayama, Y., Murtagh, D. P., Oelhaf, H., Parrish, A., Petelina, S. V., Piccolo, C., Pommereau, J., Randall, C. E., Robert, C., Roth, C., Schneider, M., Senten, C., Steck, T., Strandberg, A., Strawbridge, K. B., Sussmann, R., Swart, D. P. J., Tarasick, D. W., Taylor, J. R., Tétard, C., Thomason, L. W., Thompson, A. M., Tully, M. B., Urban, J., Vanhellemont, F., Vigouroux, C., von Clarmann, T., von der Gathen, P., von Savigny, C., Waters, J. W., Witte, J. C., Wolff, M., and Zawodny, J. M.: Validation of ozone measurements from the Atmospheric Chemistry Experiment (ACE), Atmos. Chem. Phys., 9, 287–343, doi:10.5194/acp-9-287-2009, 2009. 1692

Eriksson, P., Jiménez, C., and Buehler, S. A.: Qpack, a general tool for instrument simulation and retrieval work, J. Quant. Spectrosc. Ra., 91, 47–64, doi:10.1016/j.jqsrt.2004.05.050, 2005. 1691

Farmer, C. B.: High resolution infrared spectroscopy of the sun and the earth's atmosphere

AMTD
4, 1677–1721, 2011

from space, Mikrochimica Acta, 3, 189–214, 1987. 1683
Fischer, H., Birk, M., Blom, C., Carli, B., Carlotti, M., von Clarmann, T., Delbouille, L., Dudhia, A., Ehhalt, D., Endemann, M., Flaud, J. M., Gessner, R., Kleinert, A., Koopman, R., Langen, J., López-Puertas, M., Mosner, P., Nett, H., Oelhaf, H., Perron, G., Remedios, J., Ridolfi, M., Stiller, G. P., and Zander, R.: MIPAS: An instrument for atmospheric and climate research, Atmos. Chem. Phys., 8, 2151–2188, doi:10.5194/acp-8-2151-2008, 2008. 1683, 1684
Forster, P. M. d. F. and Shine, K. P.: Stratospheric water vapor changes as a possible contributor to observed stratospheric cooling, Geophys. Res. Lett., 26, 3309–3312, doi:10.1029/1999GL010487, 1999. 1679
Frankenberg, C., Yoshimura, K., Warneke, T., Aben, I., Butz, A., Deutscher, N., Griffith, D., Hase, F., Notholt, J., Schneider, M., Schrijver, H., and Röckmann, T.: Dynamic processes governing lower-tropospheric HDO/H_2O ratios as observed from space and ground, Science, 325, 1374–1377, doi:10.1126/science.1173791, 2009. 1683
Frisk, U., Hagström, M., Ala-Laurinaho, J., Andersson, S., Berges, J.-C., Chabaud, J.-P., Dahlgren, M., Emrich, A., Florén, H.-G., Florin, G., Fredrixon, M., Gaier, T., Haas, R., Hirvonen, T., Hjalmarsson, Å., Jakobsson, B., Jukkala, P., Kildal, P. S., Kollberg, E., Lassing, J., Lecacheux, A., Lehikoinen, P., Lehto, A., Mallat, J., Marty, C., Michet, D., Narbonne, J., Nexon, M., Olberg, M., Olofsson, A. O. H., Olofsson, G., Origné, A., Petersson, M., Piironen, P., Pons, R., Pouliquen, D., Ristorcelli, I., Rosolen, C., Rouaix, G., Räisänen, A. V., Serra, G., Sjöberg, F., Stenmark, L., Torchinsky, S., Tuovinen, J., Ullberg, C., Vinterhav, E., Wadefalk, N., Zirath, H., Zimmermann, P., and Zimmermann, R.: The Odin satellite. I. Radiometer design and test, Atronomy and Astrophysics, 402, L27–L34, doi:10.1051/0004-6361:20030335, 2003. 1688
Gettelman, A. and Webster, C. R.: Simulations of water isotope abundances in the upper troposphere and lower stratosphere and implications for stratosphere troposphere exchange, J. Geophys. Res., 110, D17301, doi:10.1029/2004JD004812, 2005. 1682, 1683
Hanisco, T. F., Moyer, E. J., Weinstock, E. M., St. Clair, J. M., Sayres, D. S., Smith, J. B., Lockwood, R., Anderson, J. G., Dessler, A. E., Keutsch, F. N., Spackman, J. R., Read, W. G., and Bui, T. P.: Observations of deep convective influence on stratospheric water vapor and its isotopic composition, Geophys. Res. Lett., 34, L04814, doi:10.1029/2006GL027899, 2007. 1682, 1683
Herbin, H., Hurtmans, D., Clerbaux, C., Clarisse, L., and Coheur, P.: $H_2^{16}O$ and HDO measurements with IASI/MetOp, Atmos. Chem. Phys., 9, 9433–9447, doi:10.5194/acp-9-9433-2009,

AMTD
4, 1677–1721, 2011

2009. 1683
Holton, J. R., Haynes, P. H., McIntyre, M. E., Douglass, A. R., Rood, R. B., and Pfister, L.: Stratosphere-troposphere exchange, Rev. Geophys., 33, 403–439, doi:10.1029/95RG02097, 1995. 1680
Hurst, D. F., Oltmans, S. J., Vö mel, H., Rosenlof, K. H., Davis, S. M.; Ray, E. A., Hall, E. G., and Jordan, A. F.: Stratospheric water vapor trends over Boulder, Colorado: Analysis of the 30 year Boulder record, J. Geophys. Res., 116, D02306, doi:10.1029/2010JD015065, 2011. 1682
Irion, F. W., Moyer, E. J., Gunson, M. R., Rinsland, C. P., Yung, Y. L., Michelsen, H. A., Salawitch, R. J., Chang, A. Y., Newchurch, M. J., Abbas, M. M., Abrams, M. C., and Zander, R.: Stratospheric observations of CH_3D and HDO from ATMOS infrared solar spectra: Enrichments of deuterium in methane and implications for HD, Geophys. Res. Lett., 23, 2381–2384, doi:10.1029/96GL01402, 1996. 1683
Johnson, D. G., Jucks, K. W., Traub, W. A., and Chance, K. V.: Isotopic composition of stratospheric water vapor: Measurements and photochemistry, J. Geophys. Res., 106, 12211–12218, doi:10.1029/2000JD900763, 2001a. 1682
Johnson, D. G., Jucks, K. W., Traub, W. A., and Chance, K. V.: Isotopic composition of stratospheric water vapor: Implications for transport, J. Geophys. Res., 106, 12219–12226, doi:10.1029/2000JD900764, 2001b. 1682
Kelly, K. K., Tuck, A. F., Murphy, D. M., Proffitt, M. H., Fahey, D. W., Jones, R. L., McKenna, D. S., Loewenstein, M., Podolske, J. R., Strahan, S. E., Ferry, G. V., Chan, K. R., Vedder, J. F., Gregory, G. L., Hypes, W. D., McCormick, M. P., Browell, E. V., and Heidt, L. E.: Dehydration in the lower Antarctic stratosphere during late winter and early spring, 1987, J. Geophys. Res., 94, 11317–11357, doi:10.1029/JD094iD09p11317, 1989. 1680, 1702
Kley, D., Russell, J. M., and Philips, C.: Stratospheric Processes and their Role in Climate (SPARC) – Assessment of upper tropospheric and stratospheric water vapour, SPARC Report 2, WMO/ICSU/IOC World Climate Research Programme, Geneva, 2000. 1680
Kobayashi, H., Shimota, A., Kondo, K., Okumura, E., Kameda, Y., Shimoda, H., and Ogawa, T.: Development and Evaluation of the Interferometric Monitor for Greenhouse Gases: a High-throughput Fourier-transform Infrared Radiometer for Nadir Earth Observation, Appl. Optics, 38, 6801–6807, doi:10.1364/AO.38.006801, 1999. 1683
Kuang, Z., Toon, G. C., Wennberg, P. O., and Yung, Y. L.: Measured HDO/H_2O ratios across the tropical tropopause, Geophys. Res. Lett., 30, 1372, doi:10.1029/2003GL017023, 2003.

AMTD
4, 1677–1721, 2011

1682, 1683
Mote, P. W., Rosenlof, K. H., McIntyre, M. E., Carr, E. S., Gille, J. C., Holton, J. R., Kinnersley, J. S., Pumphrey, H. C., Russell, J. M., and Waters, J. W.: An atmospheric tape recorder: The imprint of tropical tropopause temperatures on stratospheric water vapor, J. Geophys. Res., 101, 3989–4006, doi:10.1029/95JD03422, 1996. 1686
Moyer, E. J., Irion, F. W., Yung, Y. L., and Gunson, M. R.: ATMOS stratospheric deuterated water and implications for troposphere-stratosphere transport, Geophys. Res. Lett., 23, 2385–2388, doi:10.1029/96GL01489, 1996. 1682, 1683
Murtagh, D. P., Frisk, U., Merino, F., Ridal, M., Jonsson, A., Stegman, J., Witt, G., Eriksson, P., Jiménez, C., Megie, G., de La Noë, J., Ricaud, P., Baron, P., Pardo, J. R., Hauchcorne, A., Llewellyn, E. J., Degenstein, D. A., Gattinger, R. L., Lloyd, N. D., Evans, W. F. J., McDade, I. C., Haley, C. S., Sioris, C., von Savigny, C., Solheim, B. H., McConnell, J. C., Strong, K., Richardson, E. H., Leppelmeier, G. W., Kyrölä, E., Auvinen, H., and Oikarinen, L.: An overview of the Odin atmospheric mission, Can. J. Phys., 80, 309–319, doi:10.1139/p01-157, 2002. 1683
Nassar, R., Bernath, P. F., Boone, C. D., Gettelman, A., McLeod, S. D., and Rinsland, C. P.: Variability in HDO/H_2O abundance ratios in the tropical tropopause layer, J. Geophys. Res., 112, D21305, doi:10.1029/2007JD008417, 2007. 1682, 1689
Oltmans, S. J., Vömel, H., Hofmann, D. J., Rosenlof, K. H., and Kley, D.: The increase in stratospheric water vapor from balloonborne, frostpoint hygrometer measurements at Washington, DC, and Boulder, Colorado, Geophys. Res. Lett., 27, 3453–3456, doi:10.1029/2000GL012133, 2000. 1682
Payne, V. H., Noone, D., Dudhia, A., Piccolo, C., and Grainger, R. G.: Global satellite measurements of HDO and implications for understanding the transport of water vapour into the stratosphere, Q. J. Roy. Meteor. Soc., 133, 1459–1471, doi:10.1002/qj.127, 2007. 1682
Pollock, W., Heidt, L. E., Lueb, R., and Ehhalt, D. H.: Measurement of stratospheric water vapor by cryogenic collection, J. Geophys. Res., 85, 5555–5568, doi:10.1029/JC085iC10p05555, 1980. 1682
Randall, C. E., Rusch, D. W., Bevilacqua, R. M., Hoppel, K. W., Lumpe, J. D., Shettle, E., Thompson, E., Deaver, L., Zawodny, J., Kyrö, E., Johnson, B., Kelder, H., Dorokhov, V. M., König-Langlo, G., and Gil, M.: Validation of POAM III ozone: Comparisons with ozonesonde and satellite data, J. Geophys. Res., 108, 4367, doi:10.1029/2002JD002944, 2003. 1692
Randel, W. J., Wu, F., Russell, J. M., Roche, A., and Waters, J. W.: Seasonal cycles and QBO

AMTD
4, 1677–1721, 2011

variations in stratospheric CH_4 and H_2O observed in UARS HALOE data, Journal of Atmospheric Sciences, 55, 163–185, doi:10.1175/1520-0469(1998)055¡0163:SCAQVI¿2.0.CO;2, 1998. 1686

Ridal, M.: Water vapour isotopes in the stratosphere, Ph.D. thesis, Stockholm University, Sweden, 2001. 1682, 1683

Rinsland, C. P., Smith, M. A. H., Seals, Jr., R. K., Goldman, A., Murcray, F. J., Murcray, D. G., Malathy Devi, V., Fridovich, B., Snyder, D. G. S., and Jones, G. D.: Simultaneous stratospheric measurements of H_2O, HDO, and CH_4 from balloon-borne and aircraft infrared solar absorption spectra and tunable diode laser laboratory spectra of HDO, J. Geophys. Res., 89, 7259–7266, doi:10.1029/JD089iD05p07259, 1984. 1682

Rinsland, C. P., Gunson, M. R., Foster, J. C., Toth, R. A., and Farmer, C. B.: Stratospheric profiles of heavy water vapor isotopes and CH_3D from analysis of the ATMOS Spacelab 3 infrared solar spectra, J. Geophys. Res., 96, 1057–1068, doi:10.1029/90JD02234, 1991. 1683

Risi, C., Bony, S., and Vimeux, F.: Influence of convective processes on the isotopic composition ($\delta^{18}O$ and δD) of precipitation and water vapor in the tropics: 2. Physical interpretation of the amount effect, J. Geophys. Res., 113, D19306, doi:10.1029/2008JD009943, 2008. 1683

Rodgers, C. D.: Inverse methods for atmospheric soundings: Theory and practice, ISBN 981-02-2740-X, World Scientific Publishing Co. Pte. Ltd., 2000. 1688, 1691

Rosenlof, K. H., Chiou, E.-W., Chu, W. P., Johnson, D. G., Kelly, K. K., Michelsen, H. A., Nedoluha, G. E., Remsberg, E. E., Toon, G. C., and McCormick, M. P.: Stratospheric water vapor increases over the past half-century, Geophys. Res. Lett., 28, 1195–1198, doi:10.1029/2000GL012502, 2001. 1682

Sayres, D. S., Pfister, L., Hanisco, T. F., Moyer, E. J., Smith, J. B., St. Clair, J. M., O'Brien, A. S., Witinski, M. F., Legg, M., and Anderson, J. G.: Influence of convection on the water isotopic composition of the tropical tropopause layer and tropical stratosphere, J. Geophys. Res., 115, D00J20, doi:10.1029/2009JD013100, 2010. 1682, 1683

Scherer, M., Vömel, H., Fueglistaler, S., Oltmans, S. J., and Staehelin, J.: Trends and variability of midlatitude stratospheric water vapour deduced from the re-evaluated Boulder balloon series and HALOE, Atmos. Chem. Phys., 8, 1391–1402, doi:10.5194/acp-8-1391-2008, 2008. 1682

Schmidt, G. A., Hoffmann, G., Shindell, D. T., and Hu, Y.: Modeling atmospheric stable water

AMTD
4, 1677–1721, 2011

isotopes and the potential for constraining cloud processes and stratosphere-troposphere water exchange, J. Geophys. Res., 110, D21314, doi:10.1029/2005JD005790, 2005. 1683
Scholz, T. G., Ehhalt, D. H., Heidt, L. E., and Martell, E. A.: Water Vapor, Molecular Hydrogen, Methane, and Tritium Concentrations near the Stratopause, J. Geophys. Res., 75, 3049–3054, doi:10.1029/JC075i015p03049, 1970. 1682
Seele, C. and Hartogh, P.: Water vapor of the polar middle atmosphere: Annual variation and summer mesosphere conditions as observed by ground-based microwave spectroscopy, Geophysical Res. Lett., 26, 1517–1520, doi:10.1029/1999GL900315, 1999. 1687
Solomon, S., Rosenlof, K. H., Portmann, R. W., Daniel, J. S., Davis, S. M., Sanford, T. J., and Plattner, G.: Contributions of Stratospheric Water Vapor to Decadal Changes in the Rate of Global Warming, Science, 327, 1219–1223, doi:10.1126/science.1182488, 2010. 1679
Spang, R., Remedios, J. J., and Barkley, M. P.: Colour indices for the detection and differentiation of cloud types in infra-red limb emission spectra, Adv. Space Res., 33, 1041–1047, doi:10.1016/S0273-1177(03)00585-4, 2004. 1690, 1703
Steinwagner, J., Milz, M., von Clarmann, T., Glatthor, N., Grabowski, U., Höpfner, M., Stiller, G. P., and Röckmann, T.: HDO measurements with MIPAS, Atmos. Chem. Phys., 7, 2601–2615, doi:10.5194/acp-7-2601-2007, 2007. 1685, 1686, 1704
Steinwagner, J., Fueglistaler, S., Stiller, G. P., von Clarmann, T., Kiefer, M., Borsboom, P., van Delden, A., and Röckmann, T.: Tropical dehydration processes constrained by the seasonality of stratospheric deuterated water, Nature Geoscience, 3, 262–266, doi:10.1038/ngeo822, 2010. 1682, 1686, 1703
Stiller, G. P.: The Karlsruhe optimized and precise radiative transfer algorithm (KOPRA), Tech. rep., Wissenschaftliche Berichte FZKA 6487, 2000. 1685
Stowasser, M., Oelhaf, H., Wetzel, G., Friedl-Vallon, F., Maucher, G., Seefeldner, M., Trieschmann, O., Clarmann, T. v., and Fischer, H.: Simultaneous measurements of HDO, H_2O, and CH_4 with MIPAS-B: Hydrogen budget and indication of dehydration inside the polar vortex, J. Geophys. Res., 104, 19213–19226, doi:10.1029/1999JD900239, 1999. 1682
Tikhonov, A. N.: On the solution of incorrectly stated problems and method of regularization, Doklady Akademii Nauk (Proceedings of the Russian Academy of Sciences), 151, 501–504, 1963a. 1685
Tikhonov, A. N.: On the regularization of incorrectly stated problems, Doklady Akademii Nauk (Proceedings of the Russian Academy of Sciences), 153, 49–52, 1963b. 1685
Tikhonov, A. N. and Arsenin, V. Y.: Solutions of ill-posed problems, ISBN 0470991240, Winston

AMTD
4, 1677–1721, 2011

Publishing, New York, 1977. 1685
Urban, J., Lautié, N., Murtagh, D. P., Kasai, Y., Dupuy, E., de La Noë, J., El Amraoui, L., Eriksson, P., Frisk, U., Jiménez, C., Le Flochmoën, E., Olberg, M., and Ricaud, P.: Odin/SMR observations of stratospheric water vapour and its isotopes: Requirements on spectroscopy, in: Proceedings of the International Workshop on critical Evaluation of mm-/submm-Wave spectroscopic Data for atmospheric Observations, Irabaki University, Mito/Japan 29–30 January 2004, 2004. 1688, 1704
Urban, J., Lautié, N., Murtagh, D. P., Eriksson, P., Kasai, Y., Lossow, S., Dupuy, E., de La Noë, J., Frisk, U., Olberg, M., Le Flochmoën, E., and Ricaud, P.: Global observations of middle atmospheric water vapour by the Odin satellite: An overview, Planetary and Space Science, 55, 1093–1102, doi:10.1016/j.pss.2006.11.021, 2007. 1688
Vömel, H., Oltmans, S. J., Hofmann, D. J., Deshler, T., and Rosen, J. M.: The evolution of the dehydration in the Antarctic stratospheric vortex, J. Geophys. Res., 100, 13919–13926, doi:10.1029/95JD01000, 1995. 1680, 1702
von Clarmann, T.: Validation of remotely sensed profiles of atmospheric state variables: strategies and terminology, Atmos. Chem. Phys., 6, 4311–4320, doi:10.5194/acp-6-4311-2006, 2006. 1693
von Clarmann, T., Glatthor, N., Grabowski, U., Höpfner, M., Kellmann, S., Kiefer, M., Linden, A., Tsidu, G. M., Milz, M., Steck, T., Stiller, G. P., Wang, D. Y., Fischer, H., Funke, B., Gil-López, S., and López-Puertas, M.: Retrieval of temperature and tangent altitude pointing from limb emission spectra recorded from space by the Michelson Interferometer for Passive Atmospheric Sounding (MIPAS), J. Geophys. Res., 108, 4736, doi:10.1029/2003JD003602, 2003. 1685
Webster, C. R. and Heymsfield, A. J.: Water Isotope Ratios D/H, $^{18}O/^{16}O$, $^{17}O/^{16}O$ in and out of clouds map dehydration pathways, Science, 302, 1742–1746, doi:10.1126/science.1089496, 2003. 1682
Worden, J., Noone, D., Bowman, K., Beer, R., Eldering, A., Fisher, B., Gunson, M., Goldman, A., Herman, R., Kulawik, S. S., Lampel, M., Osterman, G., Rinsland, C., Rodgers, C., Sander, S., Shephard, M., Webster, C. R., and Worden, H.: Importance of rain evaporation and continental convection in the tropical water cycle, Nature, 445, 528–532, doi:10.1038/nature05508, 2007. 1683
Wrotny, J. E., Nedoluha, G. E., Boone, C., Stiller, G. P., and McCormack, J. P.: Total hydrogen budget of the equatorial upper stratosphere, J. Geophys. Res., 115, D04302,

AMTD
4, 1677–1721, 2011

doi:10.1029/2009JD012135, 2010. 1680

Zahn, A., Barth, V., Pfeilsticker, K., and Platt, U.: Deuterium, O^{18} and tritium as tracers for water vapour transport in the lower stratosphere and tropopause region, J. Atmos. Chem., 30, 25–47, 1998. 1682

Zahn, A., Franz, P., Bechtel, C., Grooß, J., and Röckmann, T.: Modelling the budget of middle atmospheric water vapour isotopes, Atmos. Chem. Phys., 6, 2073–2090, doi:10.5194/acp-6-2073-2006, 2006. 1683

AMTD

4, 1677–1721, 2011

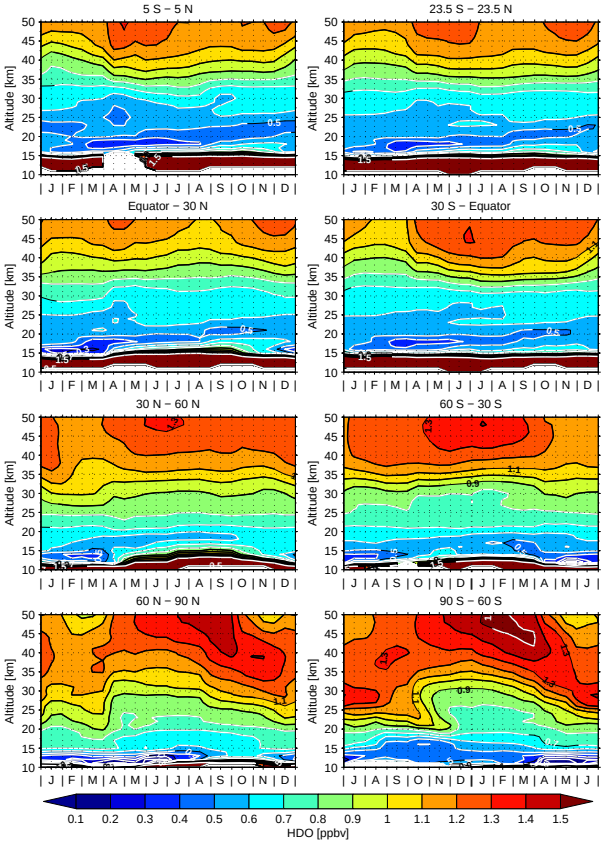

Fig. 1. Average seasonal distributions of HDO for different latitude bands derived from the Envisat/MIPAS observations between September 2002 and March 2004. Please observe that the time axis of the panels that show the annual distribution in the mid-latitudes and polar regions (last two rows) has been adjusted so that the summer season always occurs in the middle of those panels.

AMTD
4, 1677–1721, 2011

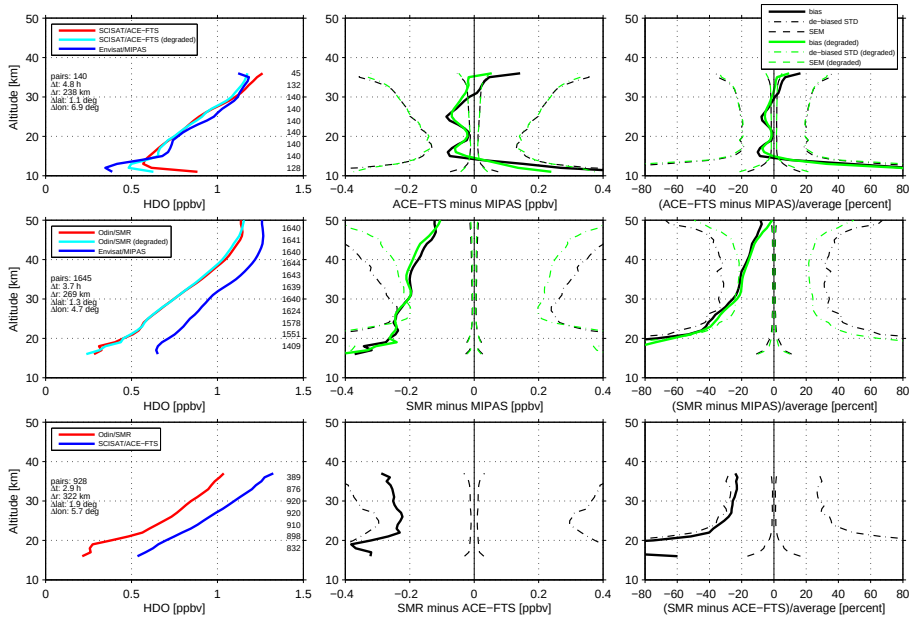

Fig. 2. Profile-to-profile comparisons of coincident HDO observations between MIPAS and ACE-FTS (upper panels), MIPAS and SMR (middle panels) and SMR and ACE-FTS (lower panels). The panels on the left-hand side show the mean profiles based on the coincident sets of data. The absolute biases are shown in the middle panels, the relative biases are given in the panels on the right-hand side. The dash-dotted lines represent the estimated combined precision of the data sets under comparison, while the dashed lines indicate the standard error of the derived biases. In the middle and right-hand panels the black lines show the results of direct comparisons, while green is used for the comparisons which involve the degradation of the vertical resolution of one data set.

AMTD
4, 1677–1721, 2011

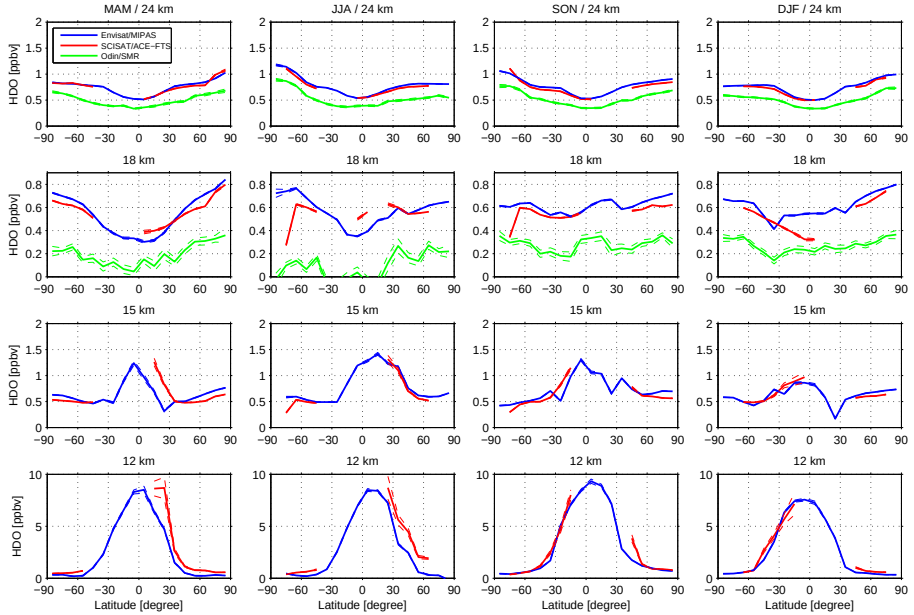

Fig. 3. Latitudinal cross sections of HDO from MIPAS (blue), SMR(green) and ACE-FTS (red) observations for different seasons and altitudes from 12 km to 24 km. The data were averaged over latitude bins of 10°. The MIPAS and SMR cross sections are based on observations from September 2002 to February 2004, for ACE-FTS the time periods September 2004–February 2006 and September 2006–February 2008 were used. Dashed lines indicate the standard error of the derived cross sections. Please mind that the y-axis range changes with altitude.

AMTD
4, 1677–1721, 2011

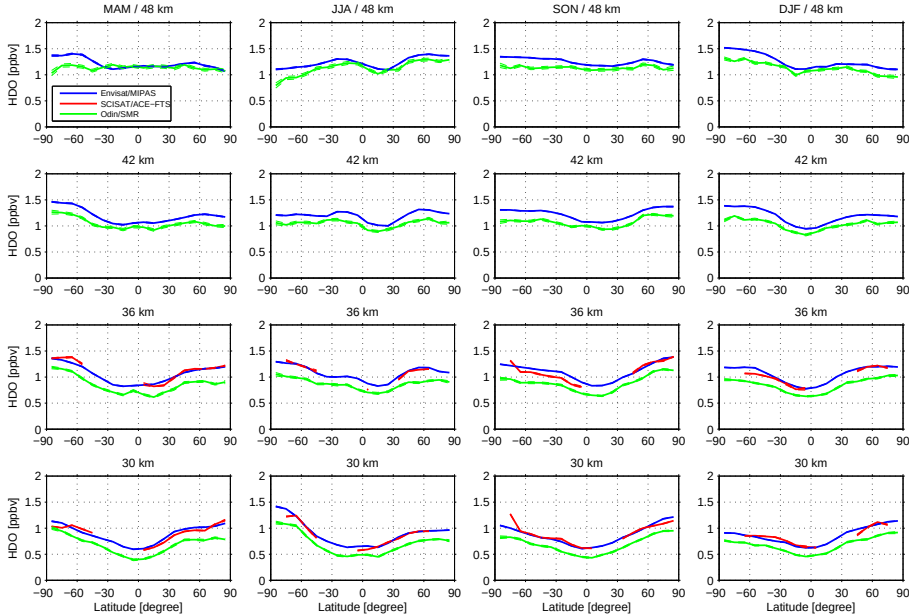

Fig. 4. As Fig. 3 but here for the altitudes from 30 km to 48 km.

AMTD
4, 1677–1721, 2011

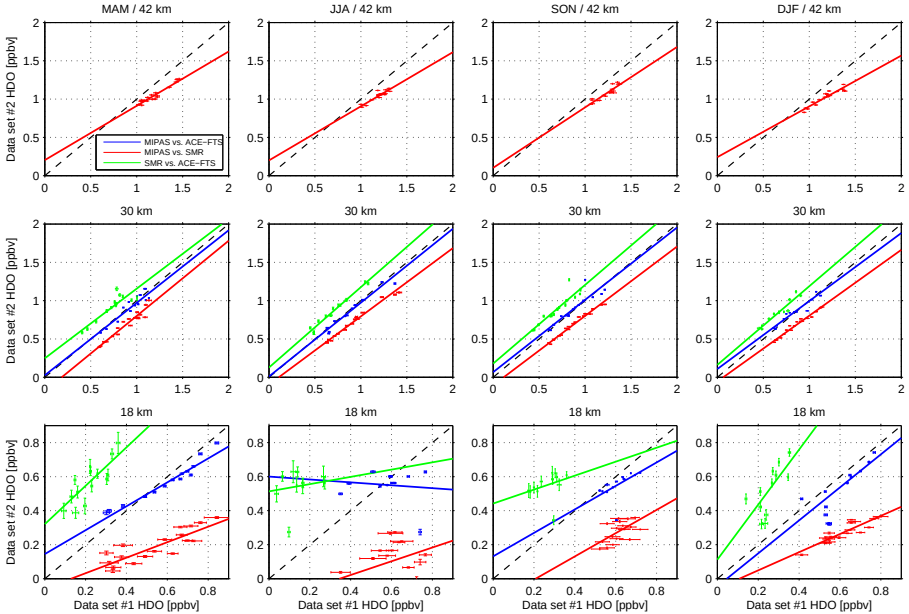

Fig. 5. Scatter plots based on the latitudinal cross sections at three representative altitudes for the different seasons. The comparison between MIPAS and ACE-FTS is shown in blue, MIPAS versus SMR is given in red while the comparison between SMR versus ACE-FTS uses green. The data set named first uses the abscissa, the latter one the ordinate. The solid lines represent the line fits for the individual comparisons. Note different scales are used for the axes depending on altitude. The dashed line gives the ideal fit.

AMTD
4, 1677–1721, 2011

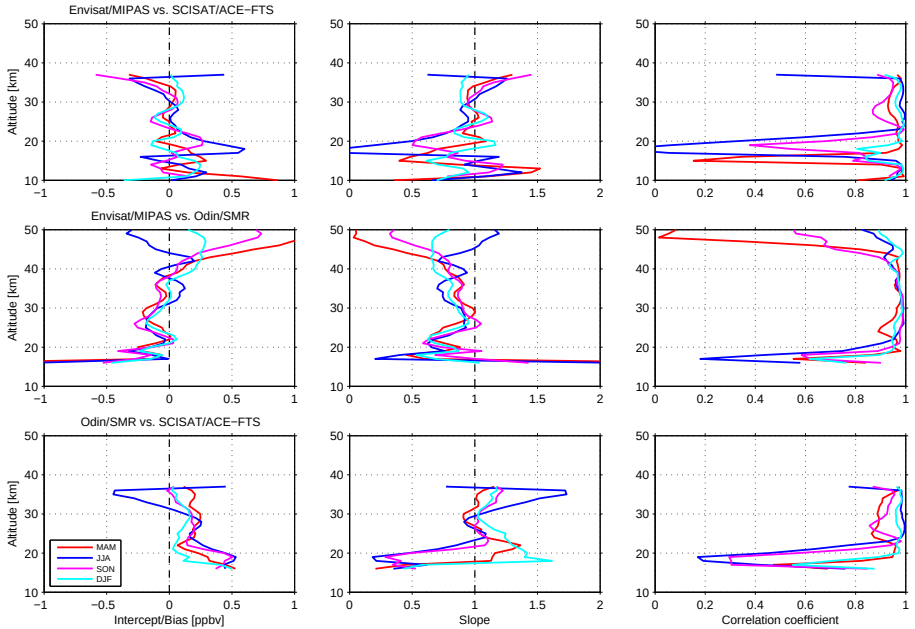

Fig. 6. Summary of the linear fit parameter and correlation coefficients derived from the seasonal comparisons of the latitudinal cross sections for the altitude range between 10 km and 50 km. The upper panels show the results for the comparison between MIPAS and ACE-FTS, the comparison between MIPAS and SMR is shown in the middle panels. The lower panels summarise the results of the comparison between SMR and ACE-FTS. The dashed lines indicate the optimal line fit parameter.

AMTD
4, 1677–1721, 2011

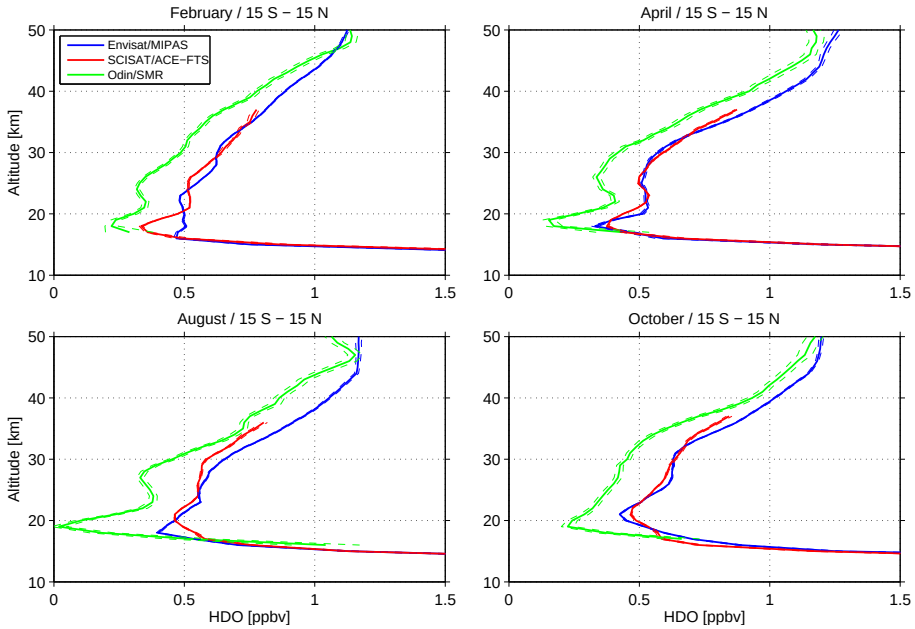

Fig. 7. Monthly mean profiles for the tropical region (15° S–15° N) for February, April, August and October. The dashed lines indicate the standard error of the mean profiles.

AMTD
4, 1677–1721, 2011